Petroleum Research 11 (2026) 815–826

Contents lists available at ScienceDirect

Petroleum Research

journal homepage: http://www.keaipublishing.com/en/journals/petroleum-research/

Full Length Article

Proppant transportation in vertical fractures with controlled roughness in different positions

Jun Li [a,*], Qingyuan Pu [a], Siyuan He [b], Mingyi Wu [b], Kewen Tang [a]

[a] State Key Laboratory of Oil and Gas Reservoir Geology and Exploitation, Southwest Petroleum University, Chengdu, Sichuan, 611630, China
[b] Sichuan Particles Energy and Technology Co., Ltd, Chengdu, Sichuan, 611630, China

ARTICLE INFO

Article history:
Received 8 September 2025
Received in revised form
9 December 2025
Accepted 22 December 2025
Available online 24 December 2025

Keywords:
Hydraulic fracturing
Controlled roughness
Roughness position
Proppant transportation efficiency
Proppant packing pattern

ABSTRACT

Effective proppant placement is essential for increasing the production of unconventional oil/gas reservoirs. It can substantially affect the fracture roughness. This paper presents a laboratory fracture model to quantify the effect of fracture roughness under well-controlled conditions. This model simulates fracture roughness by embedding particles into the walls. Via this model, the roughness can be well controlled and defined. The effect of fracture roughness location is quantified as an example to demonstrate the usefulness of the controllable fracture model. Using a fracture model with two-sided roughness, the relationships between roughness location, pump rate, and inlet location were established. The experimental results show that the rough surface in the middle resulted in a large void space in the fracture, which became more evident at a higher pump rate. This phenomenon has unexpected consequences for oil and gas production. Based on these experimental results, different sand injection modes were tested to reduce the void space caused by the surface roughness in the fractured middle. An injection mode that involves alternatively pumping proppants of different sizes was proposed to solve this problem effectively.

© 2025 Chinese Petroleum Society. Publishing services by Elsevier B.V. on behalf of KeAi Communications Co. Ltd. This is an open access article under the CC BY-NC-ND license (http://creativecommons.org/licenses/by-nc-nd/4.0/).

1. Introduction

Unconventional oil/gas reservoirs generally have lower permeability and porosity than conventional oil/gas reservoirs, making them difficult to exploit. Hydraulic fracturing technology has been widely used to exploit unconventional oil/gas reservoirs effectively. It mainly involves breaking the rock to form a fracture channel and pumping the proppant with fracturing fluid to sustain the channel (Li et al., 2022b; Zheng et al., 2022). To achieve long-term gas and oil production in reservoirs, it is necessary to ascertain the influence of critical factors on proppant transportation mechanisms and proppant placement in fracture channels (Li et al., 2022a, 2022b; Zhao et al., 2022). However, no field tool has effectively acquired proppant movement and packing patterns over the past decade. As a result, various lab-scale fracture models have been developed to understand the proppant transportation and distribution in the fracture channel of the unconventional reservoir.

Due to the difficulties in representing the rough surface in a fracture model, most of the early works used visual and vertical fracture models with smooth surfaces to test the macro-mechanisms of proppant transportation and distribution (Bello et al., 2022; Blot and Medlin, 1985; Guo et al., 2022; Kern et al., 1959; Medlin et al., 1985; Tong et al., 2018; Sievert et al., 1981). However, these tests helped elaborate on some essential mechanisms, including the proppant pile-up mechanism, the proppant movement mechanism, and the relationship between mechanisms and operational factors. Subsequently, some investigators used the CFD-DEM or CFD method to better understand the micro-mechanism of proppant transport in vertical fracture models with smooth surfaces. Their results further optimized the operational factors and revealed the relationship between the proppant transport micro-mechanism and key variables (Hu et al., 2018; Zeng et al., 2016; Zhang et al., 2017a, 2017b; Zheng et al., 2020). As mentioned above, the most widely considered proppant transportation and distribution in the fracture models are considered to have smooth surfaces. However, recent studies have

* Corresponding author.
E-mail address: lijunswpu@163.com (J. Li).
Peer review under the responsibility of Editorial Office of Petroleum Research.

https://doi.org/10.1016/j.ptlrs.2025.12.003
2096-2495/© 2025 Chinese Petroleum Society. Publishing services by Elsevier B.V. on behalf of KeAi Communications Co. Ltd. This is an open access article under the CC BY-NC-ND license (http://creativecommons.org/licenses/by-nc-nd/4.0/).

indicated that most hydraulic fractures in real-world situations have rough surfaces. More importantly, surface roughness significantly influences fluid movement and proppant placement mechanisms (Fernández et al., 2019; Kadhim et al., 2017; Liu and Sharma, 2005).

Babadagli et al. (2015) first used silica gel to copy a natural hydraulic fracture surface through casting to observe the proppant transportation and distribution mechanism in a fracture model with rough surfaces. In their study, one side of the fracture was made of opaque silicone rubber, and the other was transparent to facilitate visualization. Subsequently, several studies have been conducted to investigate proppant transportation in fracture models with rough surfaces (Huang et al., 2017; Raimbay et al., 2016). These studies used similar manufacturing methods to the one adopted by Babadagli et al. (2015). The experimental results indicated that fracture models with a rough surface significantly influenced the movements of the fracturing fluid and proppant particles. In addition, the proppant was distributed non-uniformly in a fracture model with a rough surface on one side. These previous studies have generated valuable results for understanding the influence of rough surfaces on proppant movement behavior. Recently, some investigators further developed such models, demonstrating that a two-sided rough fracture model could distinctly influence the proppant transportation and distribution (Li et al., 2021), as shown by proppant aggregation, collision, and gliding. In that study, 3D printing was used to fabricate the fracture model with two rough surfaces, which could copy the roughness of a natural hydraulic fracture surface on both sides while ensuring the visibility of the fracture model.

Li et al. (2021) highlighted the importance of considering fracture surface roughness on both sides. However, the 3D-printed fracture has certain limitations and cannot be used to fully understand the effect of fracture surface roughness. Specifically, the roughness distribution on a two-sided rough surface is random and irregular, making it difficult to replicate field fractures under controlled conditions. For instance, the position of the roughness that significantly impacts the proppant movement cannot be controlled. However, the roughness could be different because of various rock properties. Moreover, due to the complexity of manufacturing, it is difficult for interested investigators to conduct experimental studies or numerical simulations to replicate the published results based on the 3D-printed fracture model with two rough sides. These problems affect our understanding of how the two-sided rough surface influences proppant placement and must be overcome.

Therefore, this study presents a framework for simulating various fractures with well-controlled roughness. A controllable fracture model with two-sided roughness was used as an example to study the impact of roughness position on the proppant transport behavior. For this purpose, a roughness morphology of the fracture was first created from the outcrop. The value of R_a (i.e., the integral of the surface heights) was used to represent the fracture surface roughness on both sides. Then, the rough fracture surfaces ware formed by embedding a layer of packed balls with an identical radius of R_a. This method can result in quick fracture model fabrication to have anticipated roughness by controlling the packed density and ball radius. In addition, the subsequent rough surfaces can maintain consistency at different locations. With these benefits, the effect of different roughness locations on proppant placement can be studied, which has not been investigated previously. In addition, the results based on the proposed method are repeatable. In this study, the effects of the roughness location and its interaction with some key variables were studied to demonstrate the usefulness of the new method.

2. Experiment

In this study, a series of fracture models with roughness at different locations were built and utilized to study the effect of roughness location on proppant transportation and distribution. Other key variables include the pump rate and inlet location for the injection of proppant particles.

2.1. Materials

In this study, tap water was used as the fracturing fluid. The main component of the proppant was quartz sand purchased from Ao Rui material company in China. The proppant diameters were 20/40 mesh and 70/140 mesh. Meanwhile, the quartz sand was dyed dark blue for better experimental observation. From Fig. 1, the median diameters, repose angle, average and average volume density of the 20/40 mesh and 70/140 mesh proppants are 0.6 mm, 24.68°, and 2510 kg/m^3 and 0.145 mm, 35.39°, and 2480 kg/m^3, respectively. The roundness and sphericity of the different proppant sizes (20/40 mesh and 70/140 mesh) are nearly 0.6 as obtained from observing the proppant shape with a microscope (Fig. 1) and comparing it with the standard plate.

2.2. Rough fracture model

Fig. 2 schematically illustrates the experimental setup. It consists of a mixing tank with an agitator, screw pump, recycling tank, high-speed camera (1920 × 1200 resolution, **2.3 million pixels**) with a data acquisition sector (analysis software installed), LED light sources (220 V, 200 W, 400 lamp beads), and a fracture model with surface roughness at different positions.

To minimize interference from other factors in studying the relationship between the fracture roughness locations and proppant movement, the shape of the considered fracture model was simplified to rectangles. And since it simulates a tight reservoir, the model does not consider other factors such as fluid loss. Meanwhile, the widely used dynamic similarity and Reynolds number similarity criterion (Eqs. (1) and (2)) are used to guarantee consistency between the flow patterns in the experimental fracture model and those actual hydraulic fractures. Table 1 lists the dimensions of the scaled-down model, following the field data of unconventional reservoirs.

$$Q_1 A_2 / 2A_1 = Q_2 \tag{1}$$

$$\begin{cases} \mathrm{Re}_1 = \mathrm{Re}_2 \\ \mathrm{Re}_1 = \dfrac{2\rho_1 v_1 w_1 h_1}{\mu_1 (w_1 + h_1)} \\ \mathrm{Re}_2 = \dfrac{2\rho_2 v_2 w_2 h_2}{\mu_2 (w_2 + h_2)} \end{cases} \tag{2}$$

Where Q_1 and Q_2 are pump rates (m^3/min) in the field and physical model, respectively, while A_1 and A_2 are the end fracture surface areas (m^2) in the field and physical model, respectively. Re_1 and Re_2 are the Reynolds number in the field and physical model respectively. ρ_1, ρ_2, v_1, v_2, μ_1 and μ_2 the density, velocity and viscosity of fracturing fluid in the field and physical model, respectively. w_1, w_2, h_1 and h_2 are the width and height of fracture in the field and physical model respectively.

In this study, four types of fracture models were selected. In the first three cases, the rough surface was at the front, center, and rear, whereas the fourth model had a smooth surface (as shown in

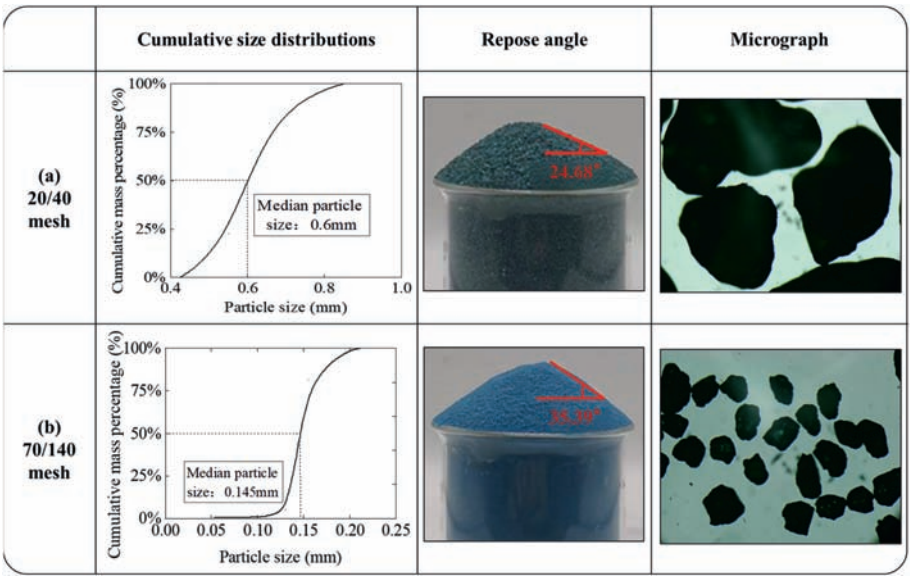


Fig. 1. Cumulative distribution curve, repose angle and micrograph of the different proppant: (a) 20/40 mesh and (b) 70/140 mesh.

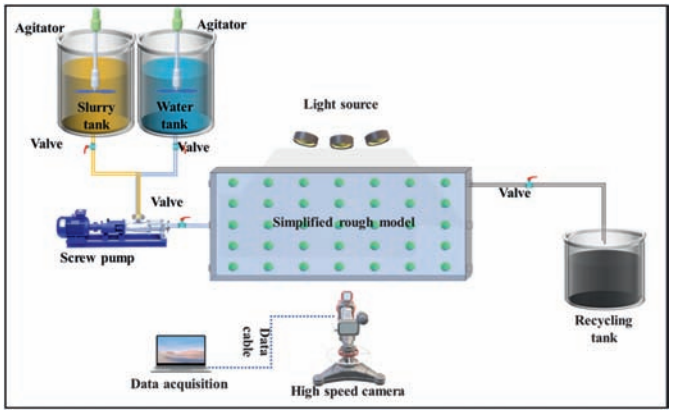


Fig. 2. Schematic of experimental system.

Fig. 3a-d). To ensure consistent roughness characteristics across different locations, we embedded small balls of identical diameter into plexiglas plates to simulate fracture roughness. We considered nine layers of closely packed balls with an identical radius and equal spacing (radius = 3 mm, vertical spacing = 10 mm, and horizontal spacing = 10 mm) to quantify the rough surfaces at different locations of the fracture models. It is worth mentioning that all the small balls were adhesively fixed into pre-dug hemispherical grooves on the transparent plexiglass plates, with only half of each sphere's volume protruding externally, and the balls are embedded in both fracture walls, resulting in two-sided roughness. (Fig. 4(b)).

Although the fracture roughness constructed by embedding spheres differs in morphology from that of actual fractures, the diameters of the spheres were designed based on realistic fracture roughness, thus ensuring that the roughness of model approximates that of actual geological formations. The above roughness morphology of the fracture models was based on the outcrop sample. We use the integral of the surface heights to quantify the natural fracture surface (Fig. 4) and the constraints in **eq. (3)**. The R_a value of the natural fracture surface considered is 1.5 mm. Hence, the packed balls with a radius of 1.5 mm are used to simulate the rough surfaces (Fig. 4(b)).

$$R_a = \frac{1}{l}\int_0^l |y(x)| d_x \tag{3}$$

where l is the sampling length and y(x) is the height of the considered points. The R_a value of the natural fracture surface considered is 1.5 mm.

Table 1
Field and experimental parameters.

Variables	Field	Lab test
Width of fracture	9 mm	9 mm
Length of fracture	200 m	200 mm
Height of fracture	100 m	100 mm
Pump rate	1–15 m^3/min	8–125 mL/s

2.3. Experimental test design

Using the experimental setup, the following steps were adopted to conduct the experiment:

(1) Selecting the fracture model and assembling the experimental system.
(2) Checking the seal of the entire system, switching on the LED light source, and properly adjusting the luminance and data acquisition system.
(3) Preparing the pad fluid and slurry.
(4) Filling up the fracture model with the pad fluid.
(5) Opening the inlet and outlet valve of the fracture model and starting recording of the experiment.
(6) Adjusting the pump to a fixed frequency and injecting the slurry into the fracture model.
(7) Stopping the experiment until all the proppant particles are used up and cleaning the experimental apparatus.

The transportation efficiency of proppant particles is considered to evaluate fracture performance. As illustrated in Fig. 5, the propped fracture area can significantly affect the oil and gas mobility. Apparently, the larger the area of proppant packing, the higher the oil/gas conductivity that can be realized. Therefore, the

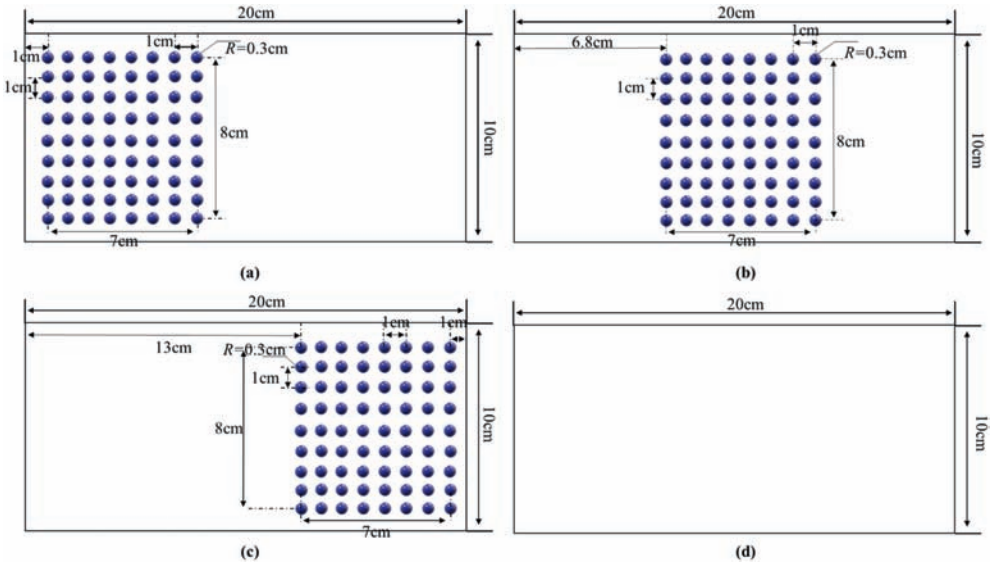


Fig. 3. Four types of fracture models: (a) rough surface at the front, (b) rough surface at the center, (c) rough surface at the rear, (d) smooth surface.

transportation efficiency of the proppant is reflected in the packing area of the proppant packing profiles. The open-source software Get-Data Graph Digitizer was adopted to determine the packing area of a proppant packing profile in this study, which is mathematically expressed as (Fig. 6):

$$S = \int_0^l f(x)d_x \tag{4}$$

where S is the packing area of the proppant packing profile, l is the length of the proppant packing bed, and $f(x)$ is the relationship between packing height and packing length.

Table 2 lists the details of 26 tests conducted in this study, where the viscosity of the fluid is 1 cp, and the proppant concentration is 3%. These results aim to demonstrate the influence of roughness position on proppant packing and transportation. The effects of the pump rate, inlet locations, and injection modes were also studied with respect to different fracture models to generate comprehensive results.

3. Results and discussion

3.1. Proppant pile up and transportation

The piling up and movement mechanisms of the proppant in the fracture model with different rough surface locations are illustrated in Figs. 7 and 8. The results of tests 1, 5, 9, and 13 (Table 2) are focused. Fig. 7 shows two stages that can be identified when the proppant piles up in the fracture model with roughness at the front. In the first stage, the proppant collision was intense when the rough surfaces were encountered as the slurry enterd the fracture, leading to a quick settlement of the proppant in the front location of the fracture model, as shown in Figs. 7 (a-1). In the second stage, when the time increases from 10s to 50s, the horizontal distance of the proppant is stable, but the height of the proppant dune increases continuously (Fig. 7 (a-2)-(a-5)). It is worth noting that after 40 s of the experiment (Figs. 7 (a-5)), the injected proppant can still flush the proppant dune surface. However, due to the roughness in the front location, the flush was weakened, leading to only a slight change in the length and height of the proppant dune later.

By contrast, the proppant packing mechanisms when the roughness is at the center and rear of the model can be classified into three stages. In the beginning, the proppant settled down quickly and formed a thin layer in the center of the fracture model (Fig. 7 (b-1) and (c-1)). This first stage occurs in the first 10–20 s, and the proppant height continues to increase. Later, in the second stage, most of the proppant settled down after entering the fracture model. As a result, the packing height of the proppant increased gradually until it reached the equilibrium height (Fig. 7 (b-4) and (c-4)). Besides, the length of the proppant dune remained unchanged in this stage. Finally, in the last stage, the subsequently injected proppant continued to flush the surface of the proppant dune, forming a hollow at the mid-front/rear location of the fracture model (Fig. 7 (b-4) and (b-5)). Overall, the proppant packing mechanism in the fracture model with smooth fracture surfaces is similar to cases where the roughness is in the center/rear. In these cases, a three-stage piling-up process is observed, similar to the works of Schols and Visser (1974) and Li et al. (2021) which also observed that the proppant accumulation within the fracture undergoes three distinct stages: initial

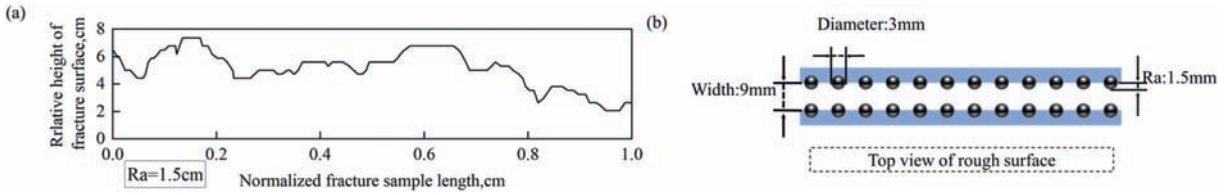


Fig. 4. (a) Roughness morphology of the outcrop sample and (b) top view of the rough surfaces in the present study.

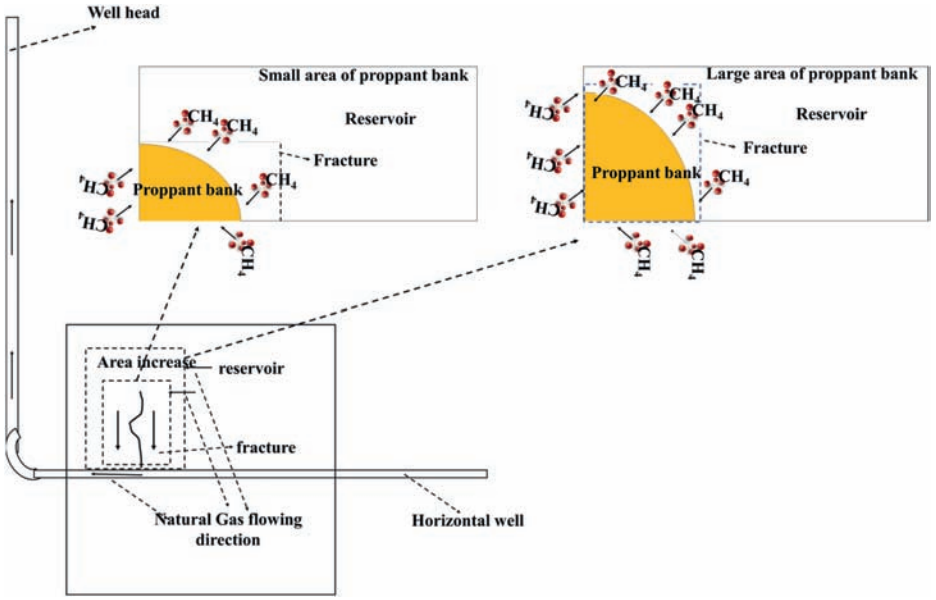


Fig. 5. Schematic illustration of the relationship between propped area and oil/gas mobility.

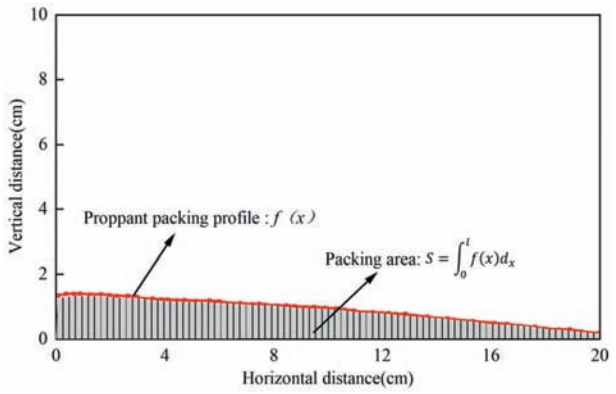


Fig. 6. Schematic illustration of the proppant packing area calculation.

length growth, followed by height growth, and subsequently further length growth.

Fig. 8 shows the variation of proppant packing area over time in the fracture model with different rough surface locations when the pump rate is 61 mL/s. It can be observed that the differences in proppant packing area over time in the fracture model with different rough surface locations are relatively small. In all cases, the proppant packing area increased almost linearly at a rapid rate during the 0–40 s period. After 40 s, the growth rate of the proppant packing area slows down significantly.

Fig. 9 presents the movement mechanism of the proppant, which differs in various fracture models. Two stages can be observed for the proppant movement when the fracture model has roughness at the front (Fig. 9 (a)). In the first stage (0–39 s), suspension and settlement were the main movement characteristics of the proppant. Subsequently, rolling and creeping were the primary movement mode in the second stage (39–55 s). Similarly, the movement mechanism of the proppant in the model with roughness at the rear and the model with smooth surfaces also has two stages. The first stage (Fig. 9 c (0–25 s) and d (0- 38 s)) was similar to the proppant behavior when the roughness was at the front of the model. However, in the second stage (Fig. 9 c (25–55 s) and d (38–55 s)), rolling, creeping, and saltation became the main movement characteristics of the proppant. The reason is that the flushing effect during proppant movement in the smooth fracture model and with rough surfaces at the rear and middle is far more significant than in the fracture model with rough surfaces at the front.

Moreover, the movement mechanism of the proppant in the fracture model with rough surfaces at the central location is

Table 2
Laboratory tests considered in this study.

No.	Roughness location	Pump rate (mL/s)	Inlet location	Injection mode
1	Front	61	Middle	Normal
2	Front	68	Middle	Normal
3	Front	83	Middle	Normal
4	Front	91	Middle	Normal
5	Middle	61	Middle	Normal
6	Middle	68	Middle	Normal
7	Middle	83	Middle	Normal
8	Middle	91	Middle	Normal
9	Rear	61	Middle	Normal
10	Rear	68	Middle	Normal
11	Rear	83	Middle	Normal
12	Rear	91	Middle	Normal
13	Smooth surface	61	Middle	Normal
14	Smooth surface	68	Middle	Normal
15	Smooth surface	83	Middle	Normal
16	Smooth surface	91	Middle	Normal
17	Front	61	Top	Normal
18	Middle	61	Top	Normal
19	Rear	61	Top	Normal
20	Smooth surface	61	Top	Normal
21	Front	61	Bottom	Normal
22	Middle	61	Bottom	Normal
23	Rear	61	Bottom	Normal
24	Smooth surface	61	Bottom	Normal
25	Middle	91 + 61	Middle	Alternative (20/40 mesh 91 mL/s, 70/140 61 mL/s)
26	Middle	91 + 61	Middle	Alternative (20/40 mesh 91 mL/s, 20/40 61 mL/s)

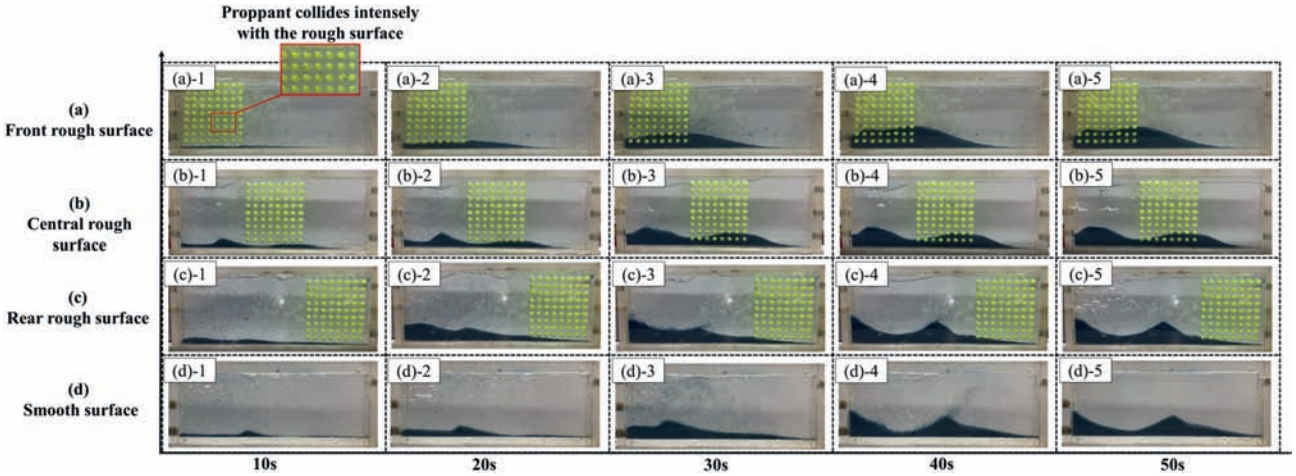


Fig. 7. Piling up of proppant in the fracture model with different rough surface locations when the pump rate is 61 mL/s: (a) front location, (b) central location, and (c) rear location of rough surfaces and (d) smooth surfaces.

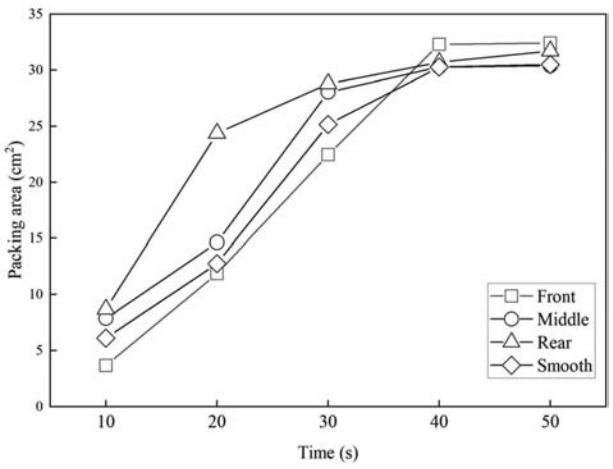


Fig. 8. The packing area of proppant in the fracture model with different rough surface locations when the pump rate is 61 mL/s at different times.

inconsistent with the previous observation (Fig. 9 b). The movement mechanism can be classified into three stages. The first stage (0–5 s) is the suspension and settlement of the proppant. In the second stage (5–47 s), the movement mode of the proppant is changed and consists mainly of saltating, rolling, and creeping at the front of the fracture model. Meanwhile, suspension and settlement also occurred at the rear of the fracture model, resulting from the roughness in the middle region. Finally, the movement of the proppant was primarily saltation and creeping in the last stage (47–55 s).

3.2. Effect of rough location

The packing pattern of the proppant in the fracture model with different locations of roughness can be illustrated in Figs. 10 and 11, corresponding to tests 1, 4, 5, 8, 9, 12, 13, and 16 in Table 2. This part considers the pump rates of 61 mL/s and 91 mL/s for proppant particles with a 20/40 mesh size. The inlet was located in the middle of the fracture model, whereas the outlet was top-oriented.

Fig. 10 shows that at a small pump rate (61 mL/s), the proppant packing pattern was wave-shaped in all the fracture models. Differently, under a high pump rate (91 mL/s), the proppant packing pattern was mainly wave-shaped in the fracture model with front and rear roughness and fracture model with smooth surface, as shown in Fig. 11. The proppant packing pattern in the centrally rough model produces an ample void space, shown as a double triangle shape packing pattern (Figs. 10 and 11).

As shown in Fig. 12, when the proppant moves to the central location in the fracture model with roughness at the center, the proppant flow is split in the middle. As a result, some proppants flowed back to the front location, and the rest flowed directly to the end location. This phenomenon requires attention as it occurs in the field of the hydraulic fracturing process, which has an arch on either side of the fracture and a void in the middle. As the confining pressure increases, the formation squeezes the fracture surface of the central void area, resulting in the closure of the hydraulic fracture and shutting down the flow channel of the hydrocarbon fluid. Therefore, it is speculated that the conductivity of oil and gas dropped dramatically. Fig. 13 illustrates this phenomenon.

Fig. 14 shows the proppant packing areas in the fracture models with rough/smooth surfaces under different pump rates (61 mL/s and 91 mL/s). The proppant packing area was the smallest when the roughness was moderate. However, the area differences were not very large for other fracture models. Therefore, it can be concluded that the proppant transportation efficiency is greatly influenced by the central roughness. There is a need of measure to overcome this problem, which will be discussed later.

3.3. Effect of pump rate

Extensive efforts have been made to reveal the effect of pump rate on the proppant transportation, packing pattern, and transportation efficiency based on smooth the fracture models. Most studies conclude that the pump rate plays a vital role in proppant packing patterns and transportation efficiency fracture models (Fernández et al., 2019; Wen et al., 2020; Xiao et al., 2021). The effects of this variable were thus studied based on the fracture models with different roughness locations. For this purpose, the pump rate changes from 61 mL/s to 91 mL/s for proppant particles with 20/40 mesh size. The inlet was located in the middle of the fracture model, and the outlet was set at the top.

Fig. 15(a)–(c), and (d) show how the proppant packing pattern changes in the models with roughness in the front and rear as well

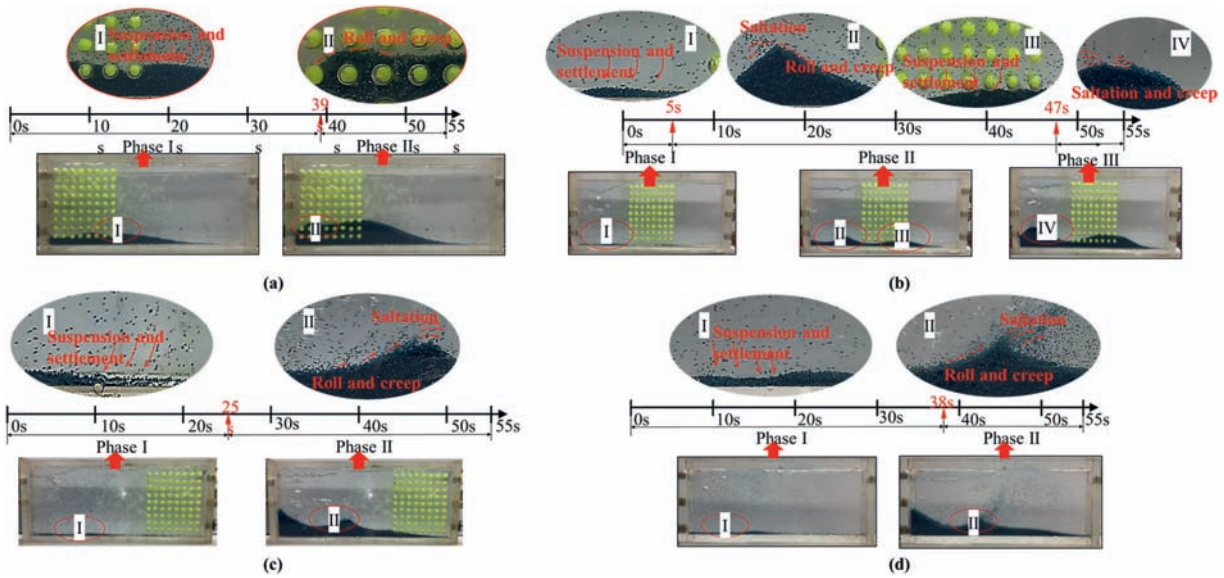


Fig. 9. Proppant movements in the fracture model with different roughness locations when the pump rate is 61 mL/s: (a) front location, (b) central location, and (c) rear location of rough surfaces and (d) smooth surfaces.

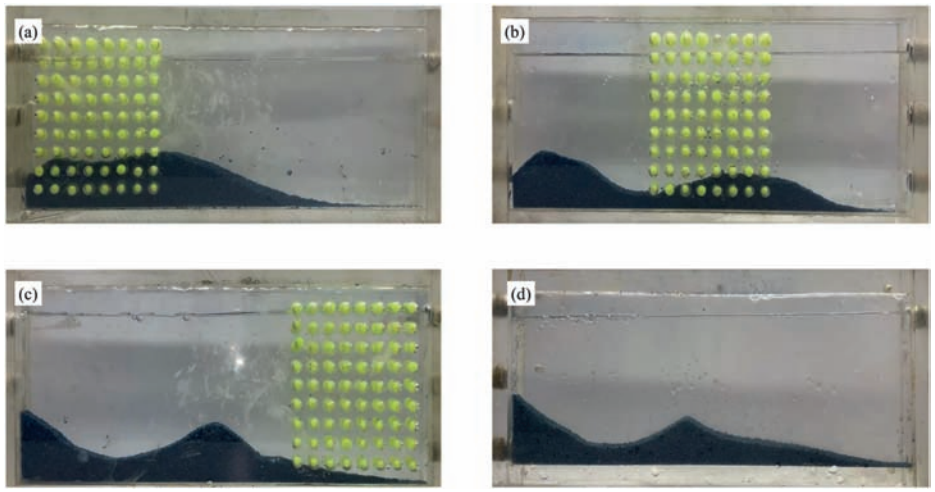


Fig. 10. Proppant packing patterns in the fracture model with different roughness locations when the pump rate is 61 mL/s: (a) front location, (b) central location, and (c) rear location of rough surfaces and (d) smooth surfaces.

as in the smooth model as the pump rate increases from 61 mL/s to 91 mL/s. A wave-shaped is generally observed under these conditions. In contrast, the packing pattern when the roughness is at the center presents a double triangle shape (Fig. 15 (b)). The latter is attributed to the split of proppant flow caused by the central roughness, as previously discussed.

Fig. 16 illustrates the proppant packing areas in the rough and smooth fracture models. With increasing pump rate, the packing area of the proppant exhibited a downward trend, irrespective of the fracture model. This trend can be explained by two reasons. One reason is that the proppant transport and movement ability are enhanced by an increased the pump rate. The second reason is that owing to the limitation in the length of these physical fracture models, more proppant is pumped out of the model when the pump rate increases from 68 mL/s to 91 mL/s, leaving less proppant in the fracture model and a smaller proppant placement area for the fracture.

Fig. 16 also shows that for the pump rates at a relatively low range (61–68 mL/s), the proppant packing area with roughness in the front of the fracture model is the highest of all. However, when the pump rate increases to the range between 69 and 91 mL/s, the proppant packing area becomes the highest in the fracture model with smooth surfaces. The main reason for this trend is that proppant particles interact with the rough front surfaces when the pump rate is low, leading to energy dissipation and the settling of proppant. The higher energy of the slurry can compensate for the energy dissipation resulting from the interactions at larger pump rates. The increased flow speed and interaction make proppant particles move more vigorously, leading to less settling in the rough fracture models than the smooth ones. Nevertheless, the proppant packing areas have insignificant differences for the fracture models with roughness in the front and rear and the smooth fracture model. However, the proppant packing area for the centrally-roughed fracture model is distinctly low at relatively high pump rates (61–91 mL/s). In other words, when the pump rate increases gradually, the effect of the central roughness becomes evident, which requires special attention.

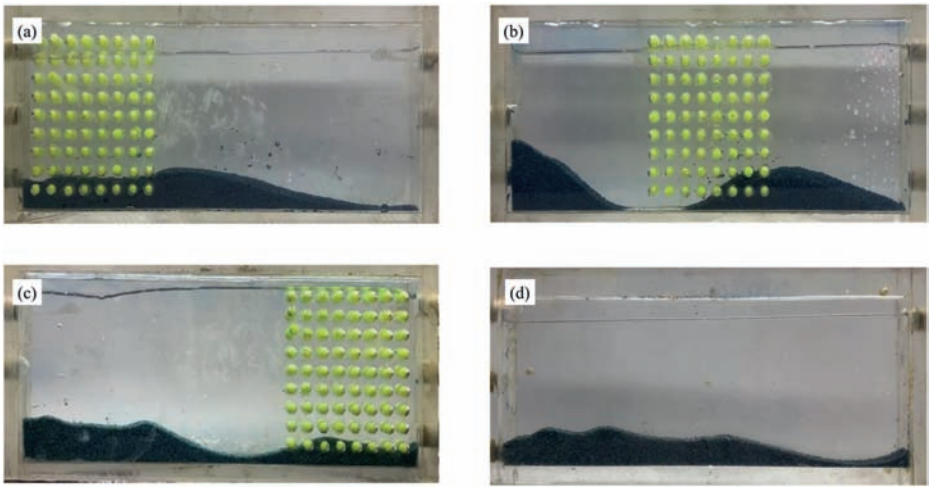


Fig. 11. Proppant packing pattern in the fracture model with different roughness locations when the pump rate is 91 mL/s: (a) front location, (b) central location, and (c) rear location of rough surfaces and (d) smooth surfaces.

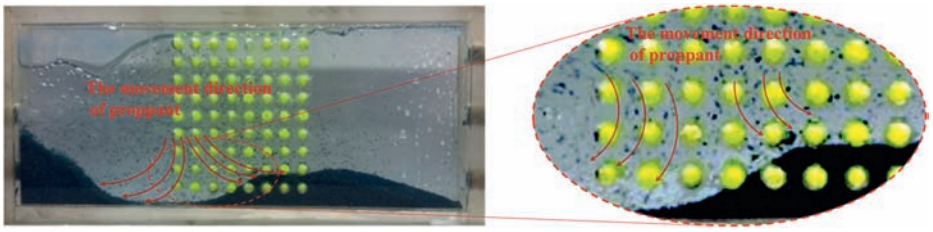


Fig. 12. Illustration of proppant movement direction in the fracture model with rough surfaces in the central region.

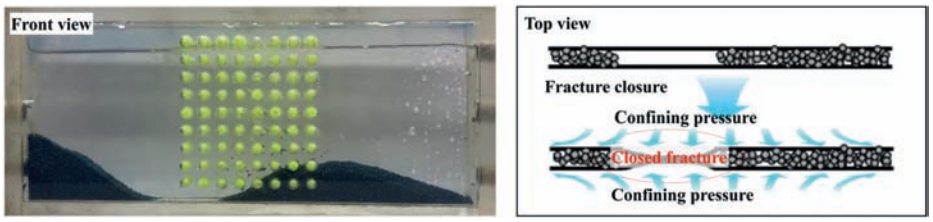


Fig. 13. Effect of void area on oil/gas flowing area under confining pressure.

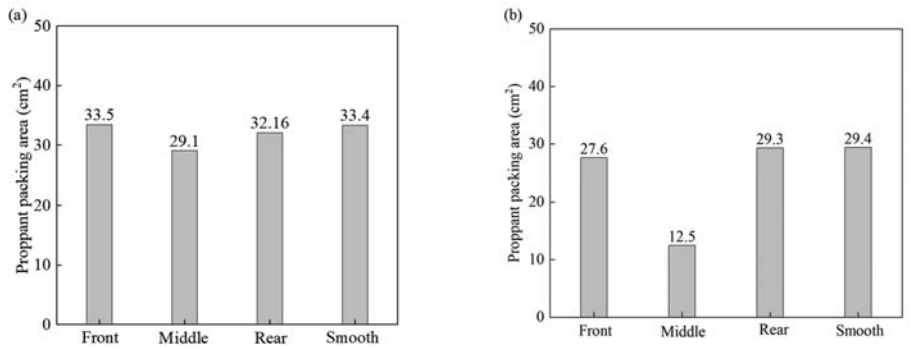


Fig. 14. Packing areas of the proppant in the fracture models with different rough surface locations at two pump rates: (a) 61 mL/s and (b) 91 mL/s.

3.4. Effect of inlet location

The inlet location for slurry injection critically affects the proppant packing pattern and transportation efficiency. This effect is also examined with respect to roughness location based on the results of tests 1, 5, 9, 13, and 17–24. Three inlet locations were considered for the pump rate of 61 mL/s and the proppant size of 20/40 mesh: top, middle, and bottom. Fig. 17 shows the final proppant packing pattern is wave-shaped in the fracture models with rough/smooth surfaces when the inlet is on the top or middle. However, when a bottom inlet location was selected, the final proppant packing pattern was triangular. Overall, the proppant placement patterns in the rough and smooth fracture models were relatively consistent regardless of the inlet injection method. They are mainly wave-shaped and triangle-shaped. However, large void areas are formed during proppant placement in fracture models with different rough surfaces using the bottom injection mode. The main reason is that when the proppant is injected from the bottom location, the injected proppant continuously flushes the surface of the proppant packing bed. Detailed information about proppant movement can be seen in Fig. 18, which decreases the flow conductivity of the fracture. Therefore, the bottom inlet position should be avoided in applications.

The variation of packing area in fracture models with rough surfaces and with smooth surfaces can be divided into two types depending on the different inlet locations (Fig. 19). In the first type, corresponding to models with roughness in the front and rear regions of the fracture, and the smooth model, as the inlet location moves from top to bottom, the packing area first increased and then decreased. In the other type with roughness, as the inlet location moved from the top to the bottom, the proppant packing area in the rough middle surface decreased significantly. However, regardless of the impact of the different inlet locations on the proppant packing area in the considered fracture models, the inflection point was always in the middle inlet locations. It is speculated that the primary reason is that the middle injection method can maintain the stable flushing effect on the surface of the proppant packing pattern, while avoiding excessive erosion of the settled proppant and a larger amount of surface settled proppant will be washed into the deeper location of the fracture (Fig. 20(a)).

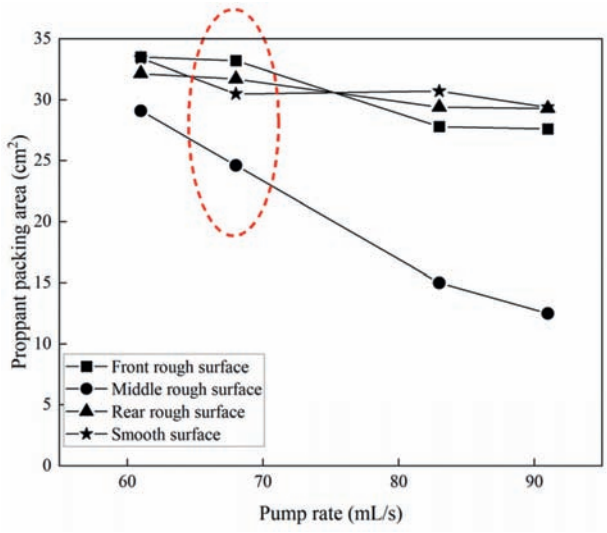


Fig. 16. Packing areas of the proppant in the fracture models with different rough surface locations at different pump rates.

In contrast, the top injection method resulted in insufficient flushing of the surface of the proppant packing pattern by the subsequently injected slurry. Thus, a little amount of surface settled proppant can be washed into the deeper location of the fracture (Fig. 20(b)). Besides, it is worth noting that the bottom injection method leads to strong flushing of the proppant near the injection point (Fig. 20(c)), thereby hindering the proppant settlement in that region and an invalid support area is generated at the front area of fracture model. Therefore, it can be concluded from the proppant placement area that middle injection is better than top injection, and top injection is better than bottom injection.

Based on the above analysis, this further indicates that the middle injection mode is preferred in field production, which can minimize the influence of the different locations of rough surfaces and improve the overall performance of the proppant transportation efficiency in hydraulic fractures.

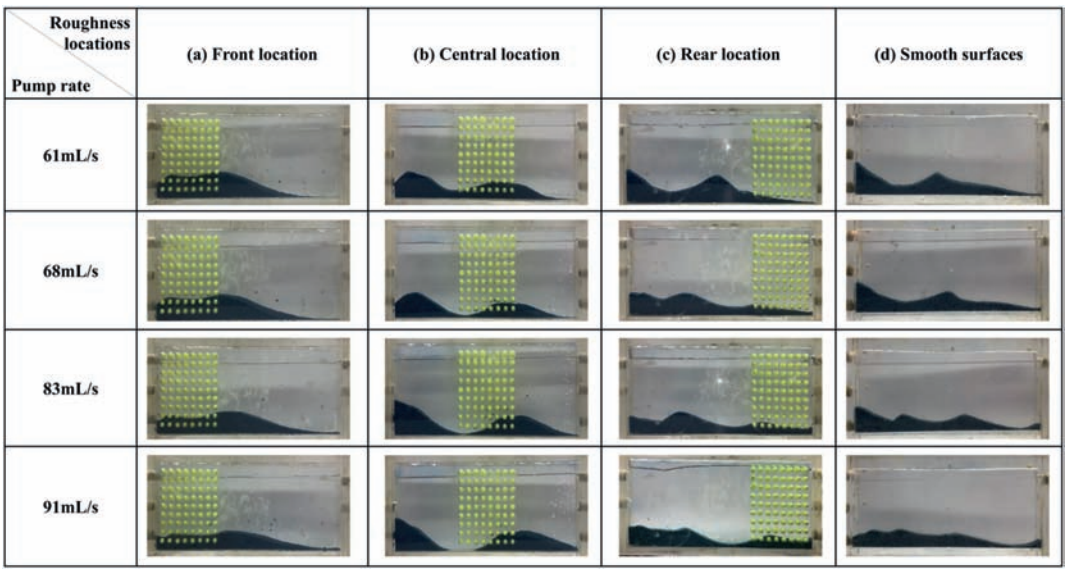


Fig. 15. Final proppant packing patterns in the fracture model with different rough surface locations at different pump rates: (a) front location, (b) central location, and (c) rear location of rough surfaces and (d) smooth surfaces.

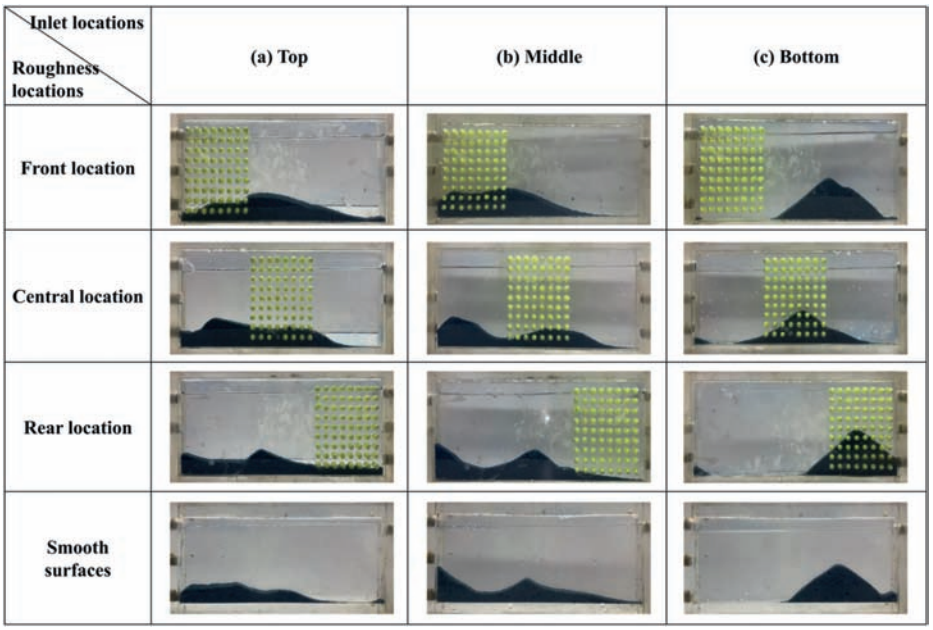


Fig. 17. Final proppant packing patterns in the fracture model with different rough surface locations under different inlet locations: (a) top inlet, (b) middle inlet, and (c) bottom inlet location.

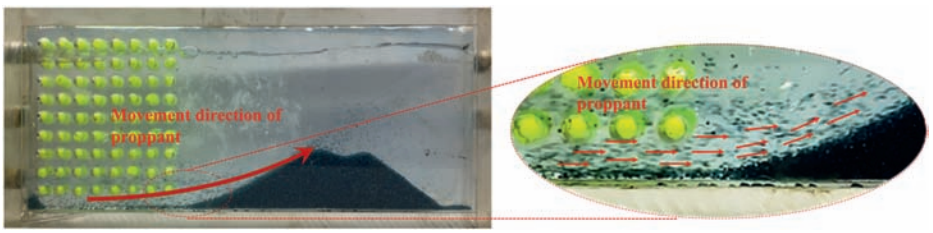


Fig. 18. Movement direction of the proppant in the fracture model with the roughness in the front using the bottom injection mode.

3.5. Measures to mitigate issues caused by wall roughness

This section tests two alternative injection modes to reduce the large void proppant packing area in the fracture model with rough middle surfaces at a high pump rate. Tests 25 and 26 in Table 2 were considered for this purpose. In these tests, the proppants of large particle size (20/40 mesh) are first pumped at a high rate (91 mL/s). Subsequently, the proppants of the same size (20/40

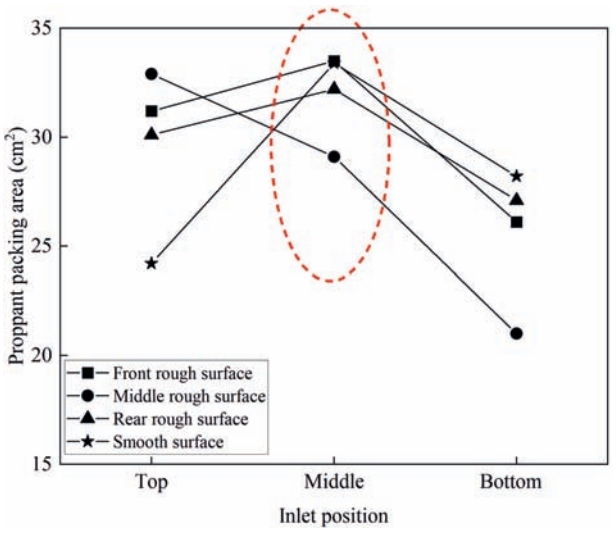


Fig. 19. Effect of inlet position on the packing area of the proppant in the fracture models with different rough surface locations.

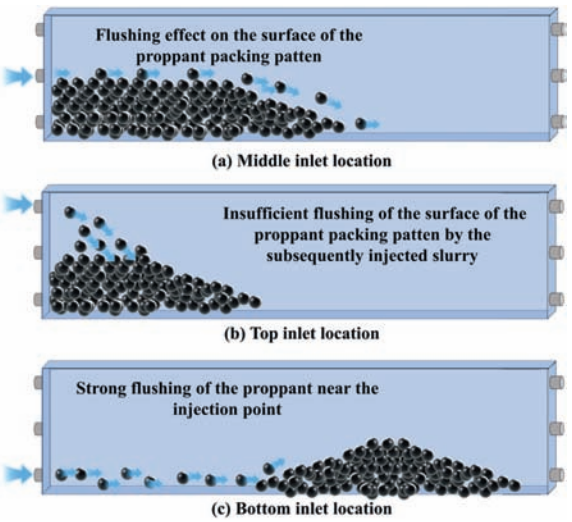


Fig. 20. Schematic diagram of different injection methods.

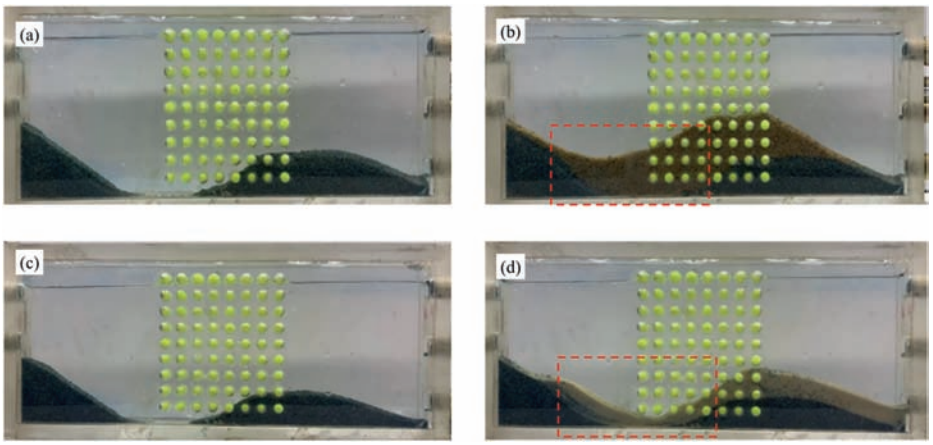


Fig. 21. Final proppant packing patterns in the central location of the fracture model with rough surfaces under different alternative injection modes: (a) injection phase I (20/40 mesh, 91 mL/s), (b) injection phase II (20/40 mesh, 61 mL/s), (c) injection phase I (20/40 mesh, 91 mL/s), and (d) injection phase II (70/140 mesh, 61 mL/s).

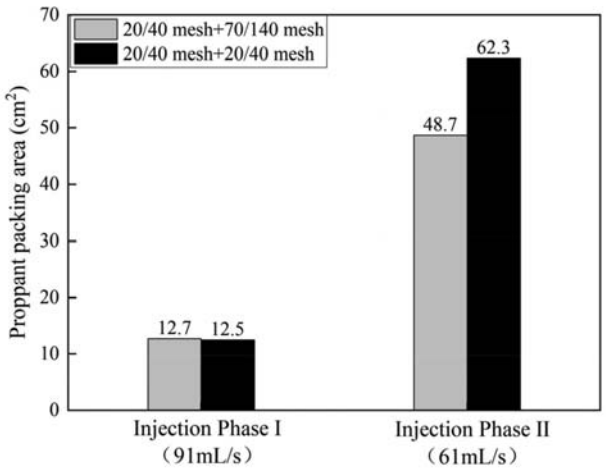


Fig. 22. Packing area of the proppant in the fracture models with different rough surface locations under different injection modes.

mesh) and small size (70/140 mesh) were pumped at a low rate (61 mL/s), respectively. In addition, the middle inlet and top outlet were selected. The results are given in Figs. 21 and 22.

The proppant packing pattern is dramatically influenced by the central roughness of the fracture model when the proppants of 20/40 mesh are pumped at a high pump rate (Fig. 21 (a) and (c)). Consequently, a large void area was generated at the central location. However, the subsequently pumped proppants of 20/40 mesh or 70/140 mesh help avoid weak areas at the central fracture location with rough surfaces (Fig. 21 (b) and (d)). Comparing the final proppant packing pattern (Fig. 21 (b) and (d)) shows that the pumped proppants of 20/40 mesh have a great filling in the void area than the 70/140 mesh. Expectedly, Fig. 22 also demonstrates that the pumped proppants of 20/40 mesh leads to a better packing area than the pumped proppants of 70/140 mesh. Therefore, it is recommended that when the impact of the roughness at the center is relatively severe, large-size proppants are injected firstly, followed by small-size proppants.

4. Conclusions

The hydraulic fractures with the rough surface affect the proppant packing pattern and transportation efficiency of unconventional reservoirs. Therefore, the influence of different rough location surfaces on proppant transport and distribution was studied in this work. In addition, the relationship between pump rate, inlet locations, injection modes, and proppant packing in the rough location surface is also discussed. It should also be noted that to better analyze the influence of roughness at different positions on the movement of the proppant, the roughness of the fracture was simplified, which led to results that were more suitable for this simplified model. The major findings are summarized as follows:

1) A vertical fracture model is designed with rough surfaces at different positions, including the front, middle, and rear of the model, which enables the simulation of surfaces with roughness at different locations. This device visualizes the proppant packing pattern and transportation efficiency at locations with different rough surfaces and considers the interaction between pump rate, inlet locations, and alternative injection modes.
2) The accumulation of proppant particles when the roughness occurs at the front surface differs from that in other fracture surfaces. However, the proppant transportation in the rough central surfaces differs vastly from that in other fracture surfaces.
3) With an increase in the pump rate, the rough surface at the center leads to ample void space in the fracture, which may reduce oil and gas production. The central inlet location should be chosen to improve the proppant packing area at different locations of the fracture model with rough or smooth surfaces.
4) When alternating proppant injection is applied, the first injection of 20/40 mesh proppants with a high pump rate (91 mL/s) leads to a severe void in the center. Subsequently, the injection mode in which proppants of the same size are injected at a low pump rate (61 mL/s) can increase the proppant bed height and enhance the proppant packing area in the fracture. This injection mode overcomes the severe void of the fracture, hereby avoiding ineffective proppant support in the fracture.

CRediT authorship contribution statement

Jun Li: Writing – original draft, Supervision, Methodology, Investigation, Formal analysis, Data curation, Conceptualization. **Qingyuan Pu:** Methodology, Investigation. **Siyuan He:** Writing – review & editing, Writing – original draft. **Mingyi Wu:**

Methodology, Investigation. **Kewen Tang:** Methodology, Investigation.

Declaration of competing interest

The authors declare no conflict of interest.

Acknowledgment

Sponsored by CNPC Innovation Found (2024DQ02-0131).

References

Babadagli, T., Raza, S., Ren, X., Develi, K., 2015. Effect of surface roughness and lithology on the water–gas and water–oil relative permeability ratios of oil-wet single fractures. Int. J. Multiphas. Flow 75, 68–81. https://doi.org/10.1016/j.ijmultiphaseflow.2015.05.005.

Bello, A., Ozoani, J., Kuriashov, D, 2022. Proppant transport in hydraulic fractures by creating a capillary suspension. J. Petrol. Sci. Eng. 208, 109508. https://doi.org/10.1016/j.petrol.2021.109508.

Blot, M.A., Medlin, W.L., 1985. Theory of Sand Transport in Thin Fluids. In: SPE Annual Technical Conference and Exhibition, Las Vegas, Nevada, USA. https://doi.org/10.2118/14468-MS.

Fernández, M.E., Sánchez, M., Pugnaloni, L.A., 2019. Proppant transport in a scaled vertical planar fracture: vorticity and dune placement. J. Petrol. Sci. Eng. 173, 1382–1389. https://doi.org/10.1016/j.petrol.2018.10.007.

Guo, J., Gou, H., Zhang, T., Zeng, X., Li, M., Tang, T, 2022. Experiment on proppant transport in near-well area of hydraulic fractures based on PIV/PTV. Powder Technology 410, 117833. https://doi.org/10.1016/j.powtec.2022.117833.

Hu, X., Wu, K., Li, G., Tang, J., Shen, Z., 2018. Effect of proppant addition schedule on the proppant distribution in a straight fracture for slickwater treatment. J. Petrol. Sci. Eng. 167, 110–119. https://doi.org/10.1016/j.petrol.2018.03.081.

Huang, H., Babadagli, T., Li, H., 2017. A quantitative and visual experimental study: effect of fracture roughness on proppant transport in a vertical fracture. In: SPE Eastern Regional Meeting, Lexington, Kentucky, USA. https://doi.org/10.2118/187520-ms.

Kadhim, D.A., Dunn-Norman, S., Imqam, A., 2017. Ceramic proppant transport and placement in heterogeneous fracture systems. In: SPE/AAPG/SEG Unconventional Resources Technology Conference. https://doi.org/10.15530/URTEC-2017-2697613. Austin, Texas, USA.

Li, H.Z., Huang, B.X., Zhao, X.L., Wu, Z.W., Jiao, X.J., Han, X.K., Sun, Z., 2022. Effects of fluid and proppant properties on proppant transport and distribution in horizontal hydraulic fractures of coal under true-triaxial stresses. J. Nat. Gas Sci. Eng. 108, 1–14. https://doi.org/10.1016/j.jngse.2022.104795.

Kern, L.R., Perkins, T.K., Wyant, R.E., 1959. The Mechanics of Sand Movement in Fracturing. J. Petrol. Technol. 11 (7), 55–57. https://doi.org/10.2118/1108-G.

Li, H., Huang, B., Zhao, X., Wu, Z., Han, X., Jiao, X., Sun, Z., 2022. Experimental investigation on proppant transport and distribution characteristics in coal hydraulic fractures under true triaxial stresses. J. Petrol. Sci. Eng. 218, 110993. https://doi.org/10.1016/j.petrol.2022.110993, 1-13.

Li, J., Liu, P., Kuang, S., Yu, A., 2021. Visual lab tests: proppant transportation in a 3D printed vertical hydraulic fracture with two-sided rough surfaces. J. Petrol. Sci. Eng. 196. https://doi.org/10.1016/j.petrol.2020.107738.

Liu, Y., Sharma, M.M., 2005. Effect of fracture width and fluid rheology on proppant settling and retardation: an experimental study. In: SPE Annual Technical Conference and Exhibition. https://doi.org/10.2118/96208-MS. Dallas, Texas.

Medlin, W.L., Sexton, J.H., Zumwalt, G.L., 1985. Sand Transport Experiments in Thin Fluids. In: SPE Annual Technical Conference and Exhibition, Las Vegas, Nevada, USA. https://doi.org/10.2118/14469-MS.

Raimbay, A., Babadagli, T., Kuru, E., Develi, K., 2016. Quantitative and visual analysis of proppant transport in rough fractures. J. Nat. Gas Sci. Eng. 33, 1291–1307. https://doi.org/10.1016/j.jngse.2016.06.040.

Schols, R., Visser, W., 1974. Proppant bank buildup in a vertical fracture without fluid loss. In: SPE European Spring Meeting. https://doi.org/10.2118/4834-MS. Amsterdam, Netherlands.

Sievert, J.A., Wahl, H.A., Clark, P.E., Harkin, M.W., 1981. Prop Transport In A Large Vertical Model. In: SPE/DOE Low Permeability Gas Reservoirs Symposium, Denver, Colorado, USA. https://doi.org/10.2118/9865-MS.

Tong, S., Singh, R., Mohanty, K.K., 2018. A visualization study of proppant transport in foam fracturing fluids. J. Nat. Gas Sci. Eng. 52, 235–247. https://doi.org/10.1016/j.jngse.2018.01.030.

Wen, H., Yang, R., Huang, Z., Zheng, Y., Wu, X., Hu, X., 2020. Numerical simulation of proppant transport in liquid nitrogen fracturing. J. Nat. Gas Sci. Eng. 84, 103657. https://doi.org/10.1016/j.jngse.2020.103657, 1-13.

Xiao, H., Li, Z., He, S., Lu, X., Liu, P., Li, J., 2021. Experimental study on proppant diversion transportation and multi-size proppant distribution in complex fracture networks. J. Petrol. Sci. Eng. 196, 107800. https://doi.org/10.1016/j.petrol.2020.107800.

Zeng, J., Li, H., Zhang, D., 2016. Numerical simulation of proppant transport in hydraulic fracture with the upscaling CFD-DEM method. J. Nat. Gas Sci. Eng. 33, 264–277. https://doi.org/10.1016/j.jngse.2016.05.030.

Zhang, G., Gutierrez, M., Li, M., 2017a. A coupled CFD-DEM approach to model particle-fluid mixture transport between two parallel plates to improve understanding of proppant micromechanics in hydraulic fractures. Powder Technol. 308, 235–248. https://doi.org/10.1016/j.powtec.2016.11.055.

Zhang, G., Li, M., Gutierrez, M., 2017b. Simulation of the transport and placement of multi-sized proppant in hydraulic fractures using a coupled CFD-DEM approach. Adv. Powder Technol. 28 (7), 1704–1718. https://doi.org/10.1016/j.apt.2017.04.008.

Zhao, Z., He, J., Guo, J., Lu, C., Yang, L., Liu, J., Liu, T., 2022. Study on proppant embedment in rough fracture surface based on three dimension laser scanning. J. Petrol. Sci. Eng. 219, 111077. https://doi.org/10.1016/j.petrol.2022.111077.

Zheng, Y., Wang, H., Li, G., Tian, G., Yang, B., Liu, M., 2022. Proppant transport characteristics in tortuous fractures induced by supercritical CO2 fracturing. Nat. Gas. Ind. B 9 (5), 457–466. https://doi.org/10.1016/j.ngib.2022.03.005.

Zheng, Y., Wang, H., Yang, B., Hu, Y., Shen, Z., Wen, H., Yan, W., 2020. CFD-DEM simulation of proppant transport by supercritical CO_2 in a vertical planar fracture. J. Nat. Gas Sci. Eng. 84, 103647. https://doi.org/10.1016/j.jngse.2020.103647, 1-14.